

Computational Evaluation of the Impact of Incorporated Nitrogen and Oxygen Heteroatoms on the Affinity of Polyaromatic Ligands for Carbon Dioxide and Methane in Metal–Organic Frameworks

Alice Henley,[†] Matthew J. Lennox,[†] Timothy L. Eason,[§] Florian Moreau,[‡] Martin Schröder,[‡] and Elena Besley^{*,†}

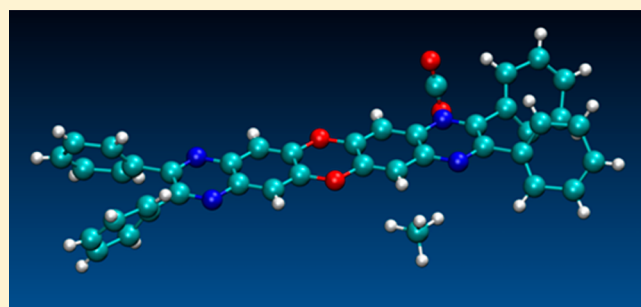
[†]School of Chemistry, University of Nottingham, Nottingham NG7 2RD, U.K.

[‡]School of Chemistry, University of Manchester, Oxford Road, Manchester M13 9PL, U.K.

[§]School of Chemistry, Cardiff University, Main Building, Park Place, Cardiff CF10 3AT, U.K.

Supporting Information

ABSTRACT: Density functional theory is employed to explore the binding of carbon dioxide and methane in a series of isorecticular metal–organic frameworks, with particular emphasis on understanding the impact of directly incorporated nitrogen and oxygen heteroatoms on the affinity of the ligand for CO₂ and CH₄. While the strongest binding sites for both CO₂ and CH₄ were found to be directly above the aromatic rings of the core of the ligand, the introduction of heteroatoms to the core systems was shown to significantly alter both the binding strength and preferred binding locations of CH₄ and CO₂. The presence of pyrazine rings within the ligand was observed to create new binding sites for both CO₂ and CH₄ and, in the case of CO₂, severely reduce the binding strength or entirely eliminate binding sites that were prominent in the analogous carbocyclic ligands. These results suggest that while the presence of framework nitrogen and oxygen heteroatoms provides a route to ligands with enhanced affinity for methane, a similar increase in affinity for CO₂ is not guaranteed.



INTRODUCTION

Metal–organic frameworks (MOFs) are a relatively new class of materials which have emerged from coordination polymer chemistry over the past few decades.¹ MOFs are constructed from inorganic secondary building units connected together using organic ligands, often creating a highly porous structure in which features such as the pore size, surface area, topology, or functionality may be controlled via judicious choice of metal and ligand.^{2–5} The tunable nature of MOFs and wide variety of accessible functionalities has resulted in their receiving a great deal of attention as high-performance adsorbents in carbon capture^{6–9} and methane storage^{10–13} technology. Computational methods play an increasingly important role in the design and evaluation of MOFs for these applications, allowing for the high-throughput screening of a vast array of candidate MOF structures.^{14–19} Computational approaches are also used in detailed exploration of particular problems such as relevant to this study, the role of coordinatively unsaturated metal sites on CO₂^{20,21} and CH₄^{22,23} adsorption, or the interaction of CH₄ and CO₂ with various organic ligands.^{24–27} In the present work, the binding of CO₂ and CH₄ with a number of real and hypothetical organic ligands inspired by the recently synthesized experimental series of metal–organic frameworks, MFM-18X,²⁸ is explored *in vacuo* using dispersion-corrected density functional theory in order to shed light on the influence of

directly incorporated heteroatomic species on ligand–guest interactions.

The MFM-18X series of frameworks (where X = 0, 1, 3, or 5) employs octacarboxylate ligands with central polycyclic cores of increasing length (Figure 1) and have been shown experimentally to exhibit promise for both CO₂ and CH₄ adsorption applications. The structures all contain three types of cavities, of which two are particularly relevant to the present work, being sufficiently large (diameter >12.4 Å) for the adsorption mechanism at low loading to be dominated by interactions between the gas and the ligand cores which form the pore walls.

While the ligands present in MFM-180 and MFM-181 are formed primarily from purely carbon-containing aromatic hydrocarbon, the ligands of MFM-183 and MFM-185 possess heteroacene cores containing additional nitrogen and, in the case of MFM-185, oxygen atoms as well. This arises from synthetic necessity; the longer ligand structures are significantly more synthetically accessible in heterocyclic form than as pure carbocycles.

Received: August 30, 2016

Revised: November 3, 2016

Published: November 18, 2016

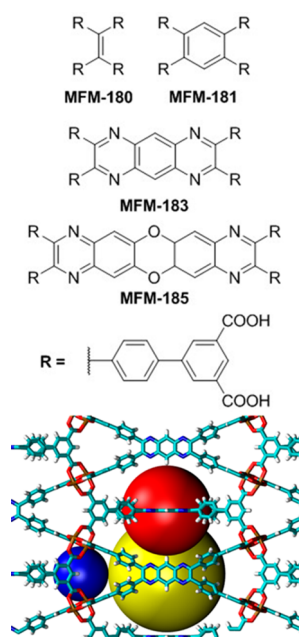


Figure 1. MFM-18X ligands as previously described (top) and the resulting three-dimensional structure, demonstrated for MFM-183 (bottom). The three different types of cavity present in the MOF are indicated by colored spheres.

The pure hydrocarbon aromatic analogues of MFM-183 and MFM-185 have proven to be synthetically unobtainable, as have both heterocyclic and carbocyclic versions of MFM-182 and MFM-184. The simulation-based approach taken in this work enables the binding mechanisms of CH_4 and CO_2 to be systematically investigated not only for the synthesized linkers used in the MFM-18X series but also for the hypothetical members of the series shown in Figure 2. This provides



Figure 2. Hypothetical linker fragments explored in this work.

significant insight into the influence of linker length and, in particular, composition on the interaction between CH_4/CO_2 and the pore walls of the framework, as well as valuable information for further experimental efforts.

RESULTS AND DISCUSSION

The interaction of single molecules of CO_2 and CH_4 with a series of organic linker fragments, based on those used in the synthesis of the MFM-18X series of MOFs, was investigated via density functional theory with Grimme 3 dispersion correction (DFT-D3)²⁹ implemented in the Q-Chem software package.³⁰ In addition to the experimentally synthesized ligand systems, the hypothetical naphthalene, anthracene, tetracene, and pentacene based ligands were also investigated.

In order to reduce the computational cost of the calculations, the isophthalic acid portions of the linkers were omitted and replaced with single hydrogen atoms (i.e., the R groups shown in Figures 1 and 2 were replaced with C_6H_5 in all simulations). The presence of electron-withdrawing functional groups (or, in the case of MOFs, the presence of a coordinated metal oxide cluster) has been shown previously to have a stabilizing effect on the guest–ligand complex.^{25,31,32} As the aromatic core of the ligand—the focus of the present study—is at least two aromatic units removed from the COOH group, however, the influence of the electron-withdrawing group on guest binding in the systems studied herein is likely to be minimal. In referring to the linker fragments studied in this work, we adopt the form L_n and $L_{n,h}$ in which n indicates the length of the central aromatic core ($n = 0$ to 5), c indicates a carbocyclic molecule, and h indicates a heterocyclic molecule.

The interaction of the guest molecule with the linker was evaluated in two steps, both using the B3LYP functional.³³ An initial geometry optimization of the guest–linker dimer was undertaken using the 6-31+G* basis set, followed by single-point energy calculations using the larger 6-311+G* basis set, from which the binding energy of the guest molecule was calculated following the counterpoise method for the correction of the basis set superposition error.³⁴ Partial charges were determined using the CHELPG method.³⁵ For each guest–linker system, several initial geometries were evaluated, and in all calculations the atoms of the linker fragment were kept fixed, while the guest molecule and its constituent atoms were allowed to adjust position upon optimization.

In order to validate the adopted computational methodology, a range of benchmarking calculations were performed for a simple weakly interacting system: the CO_2 – C_6H_6 dimer. These results are compared with the literature values for the binding energy and equilibrium separation obtained by coupled-cluster theory with iterative singles-and-doubles excitations and a perturbative treatment of triplet excitations, CCSDT(T), in the limit of the complete basis set (CBS)³⁶ as well as other available data. Table 1 summarizes a comparison between the performance of the B3LYP-D3 method, used in this study, with the CCSD(T) method and less accurate Møller–Plesset Perturba-

Table 1. Benchmarking Results for the Binding Energy and Equilibrium Distance in CO_2 – C_6H_6 Dimer Comparing the Performance of B3LYP-D3, MP2, and CCSD(T) Methods

method	basis set	R (Å)		binding energy (kJ/mol)
configuration A				
MP2 ³⁹	def2-QZVPD	3.35 ^a		−11.90
	def2-TZVPD	3.35 ^a		−9.90
B3LYP-D3	def2-QZVPD	3.28		−10.41
	def2-TZVPD	3.28		−10.29
B3LYP-D3	6-31+G*	3.28		−10.24
CCSD(T) ³⁶	CBS	3.25		−10.20 ± 0.40
CCSD(T) ³⁹	CBS	3.35 ^a		−10.70
CCSD(T) ³⁹	aug-cc-pVTZ	3.35 ^a		−9.70
configuration B				
MP2 ³⁹	def2-QZVPD	2.769	2.772	−4.00
B3LYP-D3	def2-QZVPD	2.69	2.70	−5.42
	def2-TZVPD	2.69	2.70	−5.32
B3LYP-D3	6-31+G*	2.71	2.71	−4.96

^aGeometry optimized at the MP2/Def2-TZVPP level of theory.

tion theory, MP2. For both configurations of CO₂–C₆H₆ dimer, “stacked” (configuration A in Figure 3) and “end on”

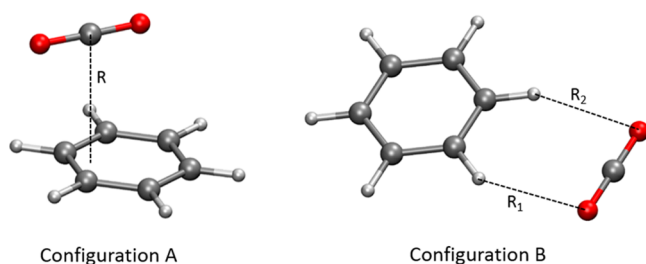


Figure 3. Two configurations of CO₂–C₆H₆ dimer used in benchmarking calculations presented in Table 1.

(configuration B in Figure 3), B3LYP-D3 results perform consistently better than MP2 and, in the case of configuration A, are in excellent agreement with the “golden standard” CCSD(T)/CBS results.

A very good agreement for the binding energies calculated using CCSD(T) and DFT-D3 methods has been previously reported³⁷ for noncovalent interactions of CO₂ molecule with a large set of organic linker molecules including nitrogen-containing heterocycles. The authors³⁷ concluded that both methods are suitable tools to study such weakly bound systems. The performance of B3LYP-D3 hybrid functional augmented with a dispersion term has been also shown to be reliable for description of the interaction between small molecular adsorbates (CH₄, H₂, N₂, CO₂, CO, H₂O, and NH₃) with Cu- and Fe-containing coordinatively unsaturated sites (CUSs), with the root-mean-square deviation (RMSD) values being typically below 3 kJ/mol.^{20,38}

In the case of the nonheterocyclic linkers (L0_c, L1_c, L2_c, L3_c, L4_c, and L5_c), a steady increase in binding strength is observed as the linker length is decreased, reaching a maximum for L1_c (Figure 4, top). For both CH₄ and CO₂, the highest strength binding locations on the carbocyclic linkers were found to be adjacent to the phenyl rings on each end of the linker, either directly over or near the first aromatic ring of the carbocycle (Figure 4, bottom). The primary interaction in this location is between either a positively charged hydrogen (in the case of CH₄) or carbon atom (for CO₂) with the electron-rich center of the aromatic ring. Additional, weaker interactions exist between the guest molecule and the edges of nearby terminal phenyl groups. As the separation between the terminal phenyl groups is reduced by removing aromatic units from the center of the linker, guest molecules are able to interact not only with the nearest pair of phenyl rings but also with those on the opposite end of the linker, resulting in the observed increase in binding strength. Further reduction in linker length from L1_c to L0_c eliminates the central aromatic component of the linker entirely and results in increased steric hindrance due to the short separation between terminal phenyl groups, forcing the guest molecule further away from the linker (Figure 4, bottom). As a result of these two factors, both CH₄ and, in particular, CO₂ were found to be much more weakly bound in L0_c than in L1_c (Figure 4, top).

While guest binding on the preferred binding site within the carbocyclic linker series—the aromatic ring nearest the phenyl groups—is weakened as the linker is extended, the introduction of additional aromatic rings results in an increase in the total number of viable binding sites. In the case of CH₄, additional

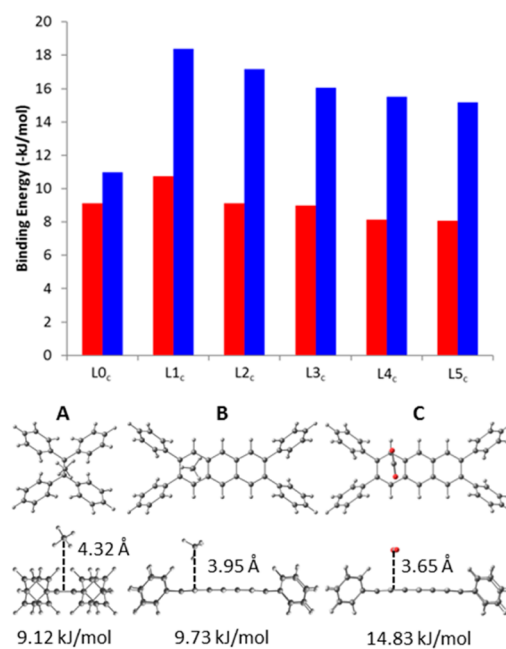


Figure 4. Calculated binding energy (top) of CH₄ (red) and CO₂ (blue) in the nonheterocyclic linkers and representative preferred binding sites (bottom) viewed from above and the side of the linker fragment: (A) CH₄ on L0_c; (B) CH₄ on L3_c; (C) CO₂ on L3_c.

binding sites were found both directly above any additional aromatic rings and above the C–C aromatic bonds shared by adjacent rings (Figure 5). The secondary binding sites were

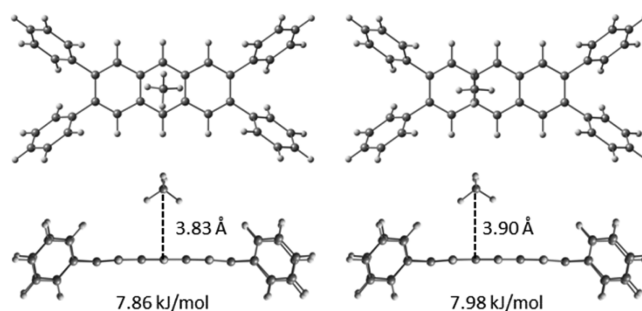


Figure 5. Representative secondary CH₄ binding sites on L3_c viewed from above and the side of the linker fragment. Similar binding modes were observed on L4_c and L5_c (see Supporting Information).

found to exhibit very similar binding energies (within 0.2 kJ/mol of each other) but were all found to be approximately 1 kJ/mol (~10%) weaker than the primary binding location for each linker. It should be noted that while these sites are viable in terms of binding energy, many are likely to be mutually exclusive and, particularly in the shorter L0_c–L2_c systems, the presence of more than one CH₄ molecule on each face of the ligand may be sterically impossible. Given the similarity in binding energies observed along the core of the ligand, it is unlikely that CH₄ will remain localized on one particular site under ambient conditions, and the interaction energy in the real system is therefore likely to be an average of both primary and secondary sites.

Little difference was observed in methane binding energy with the secondary binding sites on extension of the linker system from L3_c to L4_c and L5_c, indicating that while an increase in linker length results in a more weakly bound

methane molecule at the primary adsorption site, it is not detrimental to the adsorption of methane on secondary sites. The inclusion of a longer ligand is therefore likely to be advantageous, allowing more than one methane molecule to bind with the same ligand without the steric clashes between primary and secondary sites that exist in $L0_c$ – $L2_c$, although a full exploration of the many-molecule system would require a classical statistical mechanics approach.

In the case of CO_2 , secondary binding sites were also observed either directly over any additional aromatic rings present in the linker or over a shared aromatic C–C bond. CO_2 was always found to align itself with the O–C–O axis parallel to the plane of the aromatic core of the linker and generally adopted a position with the O–C–O axis either aligned with or perpendicular to the long axis of the aromatic core (Figure 6).

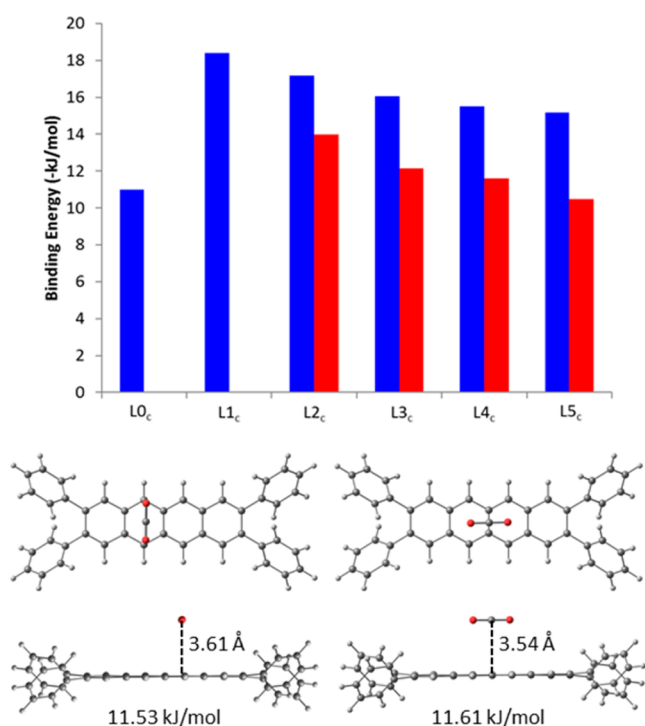


Figure 6. Dependence of CO_2 –linker binding energy on linker length for primary (blue) and secondary (red) binding sites (top) and representative secondary binding sites for CO_2 on $L4_c$ (bottom). Similar binding modes were observed for $L3_c$ and $L5_c$ (see Supporting Information). $L0_c$ and $L1_c$ do not contain enough aromatic rings to allow for secondary binding sites.

Unlike methane, however, CO_2 binds much more weakly to the secondary sites when compared to the primary binding locations and a steady decrease in binding strength is observed for secondary sites as the linker is extended (Figure 6), a result of the more significant electrostatic interactions between CO_2 and the phenyl rings at the end of the linkers, which remains non-negligible at a longer separation distance than the primarily dispersive CH_4 –linker interactions.

While both CH_4 and CO_2 behave similarly in the non-heterocyclic linkers with respect to the available binding sites and dependence of binding energy on linker length, the same is not true upon introduction of N- and O-heteroatoms to the system, such as those present in $L3_h$ and $L5_h$. The presence of nitrogen and oxygen within the aromatic core of the linker alters the distribution of charge in the system, introducing

regions of significant positive charge (Figure 7). This has the effect of both creating new viable binding sites and significantly altering—and even eliminating—previously identified sites.

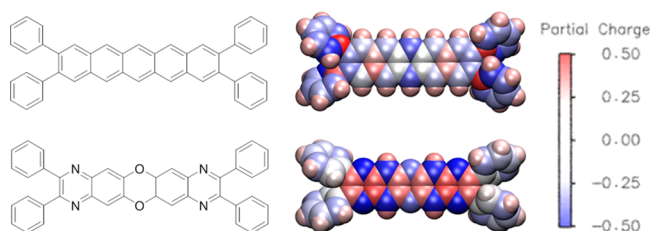


Figure 7. Comparison of CHELPG partial charge maps of the carbocyclic (top) and heterocyclic (bottom) forms of $L5$. A similar change in charge distribution was observed for $L3$ (see Supporting Information).

In the case of the heterocyclic $L3_h$ linker, the preferred methane binding site was found to be directly over the pyrazine rings of the linker, near the outer phenyl groups, with a binding energy of 8.50 kJ/mol (Figure 8). Further viable binding

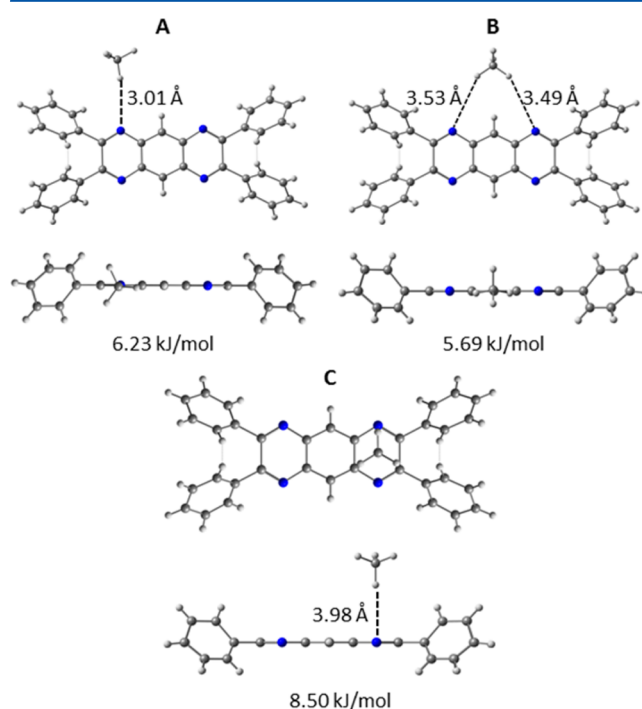


Figure 8. Binding sites identified for the CH_4 – $L3_h$ dimer: (A, B) secondary binding sites created via C–H...N interactions; (C) preferred binding site above a pyrazine ring.

geometries were observed along the sides of the linker, in which the hydrogen atoms of the methane molecule are able to form weak hydrogen bondlike interactions via directed C–H...N interactions (Figure 8). While the interaction between methane and the side of the linker (binding energies between 5.69 and 6.23 kJ/mol) are 2–3 kJ/mol weaker than the interactions observed between methane and the π system of the rings, they still exceed kT at room temperature, suggesting that they do represent viable methane adsorption sites. Methane was not observed to bind along the edge of the linker in the carbocyclic analogue, $L3_c$. While the introduction of N-heteroatoms to the $L3$ system causes methane to be slightly less strongly bound on

locations above the ring system, the creation of additional binding sites via hydrogen bonding suggests that the heterocyclic linker is a more attractive candidate for low-pressure methane adsorption than its carbocyclic equivalent. Furthermore, since methane molecules bound directly above the aromatic core and via weak hydrogen bonding on the edges of the ligand are unlikely to introduce any steric clashes, the inclusion of heterocyclic ligands introduces the potential for cooperative methane binding, such as that observed in the case of some functionalized benzene systems.⁴⁰

While the location of the strongest methane binding sites on the carbocyclic L3_c and heterocyclic L3_h linkers remained very similar, the introduction of additional O-heteroatoms in the longer L5_h linker significantly alters the preferred CH₄ binding locations. For the CH₄-L5_h system, the strongest interactions were observed when methane was located directly above the oxygen-containing, electron-rich central ring of the linker (Figure 9). Although a similar configuration was observed in

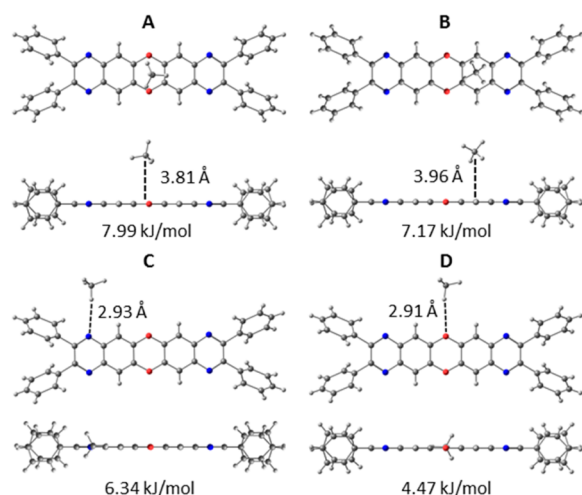


Figure 9. Binding sites identified for the CH₄-L5_h dimer: (A, B) preferred binding sites above or next to the oxygen-containing ring; (C, D) secondary binding sites along the side of the linker.

the carbocyclic L5_c, methane exhibits a noticeably stronger interaction with the heterocycle (by between 0.5 and 0.9 kJ/mol). In contrast to the L3_h system, no dimers were observed in which methane is bound above the plane of the pyrazine rings of L5_h (cf. Figure 8C for L3_h), suggesting that the outer phenyl rings play a role in stabilizing the bound methane in the shorter L3_h ligand. As in L3_h, the interaction between H of CH₄ and the heteroatoms of the linker creates a number of new methane binding sites in comparison to the carbocyclic analogue, L5_c (Figure 9). The strongest of these new sites are located near the N-heteroatoms (BE = 6.34 kJ/mol; Figure 9C), a result of the interaction between C-H and the nitrogen lone pair. Further sites are located near the O-heteroatoms, either via a direct C-H...O interaction (BE = 4.47 kJ/mol; Figure 9D) or a bridging mode, in which methane is seen to interact weakly with both nitrogen and oxygen (BE = 4.76 kJ/mol; Supporting Information). As in L3_h, the binding energies for these newly created sites exceed *kT* at room temperature, indicating that they can be expected to play a non-negligible role in methane adsorption at low pressure.

The introduction of heteroatoms was found to have an even greater impact on the binding of CO₂ with the L3 and L5 systems. The change in charge distribution induced by the

introduction of O and N atoms to the linker significantly reduces the affinity of the region above the rings for CO₂. Whereas the strongest interactions in the carbocyclic L3_c and L5_c were found to be directly over the ring systems (BE = 16.06 and 15.17 kJ/mol, respectively), only comparatively weak interactions (about 7–12 kJ/mol) were found for similar conformations in the heterocyclic systems. As was the case for methane, several new strong CO₂ binding sites were identified near the N-heteroatoms (Figure 10), exhibiting binding

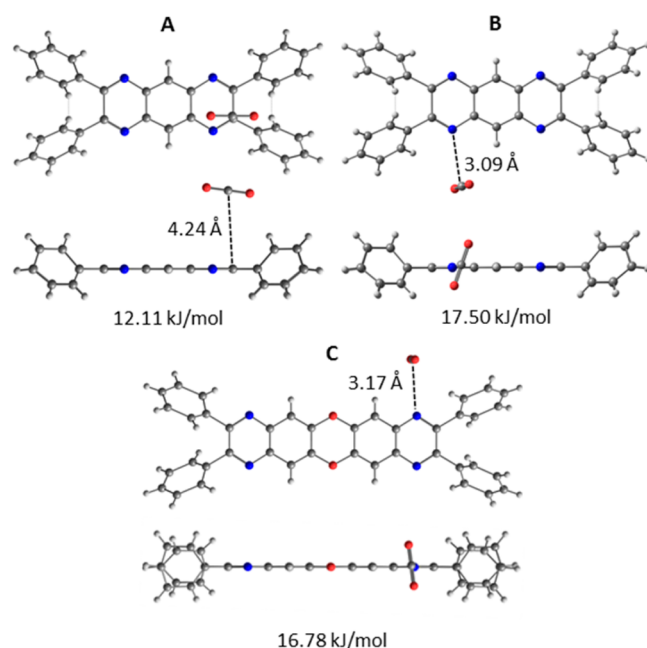


Figure 10. Representative binding sites for CO₂ on the heterocyclic L3_h and L5_h linkers: (A) comparatively weak interaction with the pyrazine rings of L3_h (4 kJ/mol weaker than equivalent sites in L3_c); strongest binding site (B) on L3_h; (C) on L5_h, created via C_{CO₂}...N and O_{CO₂}... π interactions.

energies of around 17.5 kJ/mol (L3_h) and 16.7 kJ/mol (L5_c), approximately 1–2 kJ/mol stronger than any sites observed in their carbocyclic analogues. The CO₂ molecule is able to bind strongly with the linker via a combination of the interaction of the positively charged C of CO₂ with the negatively charged N-heteroatoms and interactions between the negative O of CO₂ and the regions of slight positive charge above and below the ring. The overall effect of heteroatoms on the adsorption of CO₂ in these systems is likely to be minimal, however, as the introduction of new binding sites along the sides of the linker is to a certain extent, counterbalanced by the elimination of binding sites above and below the aromatic core.

From the point of view of the selective adsorption of CO₂ over CH₄ at low loading—in which the selectivity is dominated by the interaction of the two species with the framework—the ratio of the binding energies of the two components (BE_{CO₂}/BE_{CH₄}) is of greater interest than the binding energies themselves. In the case of primary adsorption sites on non-heterocyclic linkers, CO₂ always binds more strongly with the linker than CH₄, and the ratio from the calculations was found to vary from 1.21 (in L0_c) to a maximum of 1.91 (in L4_h). Little dependence of the ratios of binding energies of the five carbocyclic linkers on linker length was observed, with the lowest ratios being observed in L1_c and L3_c (1.71 and 1.79,

respectively), while the ratios in the remaining three linkers ranged from 1.88 to 1.91. When both primary and secondary binding sites are considered, the selectivity of linkers L1_c through L5_c was found to be almost identical, with binding energy ratios ranging from 1.63 (L5_c) to 1.72 (L4_c). The presence of heteroatoms in the linkers appears to be beneficial to CO₂ selectivity when sites along the sides of the linkers are considered ($BE_{CO_2}/BE_{CH_4} = 2.67\text{--}2.91$). Although CO₂ is expected to be selectively bound over CH₄ along the edges of the heterocyclic linkers, the redistribution of charge above and below the aromatic core of the linker is detrimental to CO₂, and methane is preferred in sites above the ring system of L3_h as a result ($BE_{CO_2}/BE_{CH_4} = 0.82$).

CONCLUSIONS

In this work, we have presented an extensive computational study of the binding of CH₄ and CO₂ with a series of real and hypothetical MOF ligands, exploring the effect of linker length and the presence of N- and O-heteroatoms on the affinity of the linker for the two species. It has been shown that the strongest binding sites for both CH₄ and CO₂ in the carbocyclic linkers are found directly above the aromatic rings of the linker core, primarily the ring nearest to the outer phenyl rings of the system. The strongest binding on the carbocyclic linkers were observed for the benzene and naphthalene based systems, in which strong interactions with the π system of the aromatic rings are combined with additional interactions with the nearby outer phenyl rings. The shortest linker, L0_c, was found to introduce significant steric restrictions on the binding locations of CH₄ and CO₂, and both species were only weakly bound as a result.

Although the introduction of heteroatoms to the linkers was found to be beneficial in the case of CH₄, the case was not as clear for CO₂. In the heterocyclic linkers, CH₄ was able to bind in the regions above and below the heterocyclic core of the linker with only a small reduction in binding strength compared to the carbocyclic analogues. The presence of heteroatoms introduced additional adsorption sites along the sides of the heterocycle, a result of hydrogen-bond-like interactions between methane and the heteroatoms, presenting an attractive route to increased CH₄ adsorption affinity in MOFs with polyaromatic ligand systems, particularly when combined with proposed methods toward frameworks containing linkers with increased aromatic surface area.^{18,41,42}

The presence of heteroatoms in the L3_h and L5_h linkers was found to significantly enhance CO₂ binding compared to the carbocyclic L3_c and L5_c. The strongest binding sites, however, were found to be along the sides of the heterocycle, and CO₂ was no longer able to bind strongly with sites above and below the aromatic core. The effect of incorporation of heteroatoms into MOFs on CO₂ adsorption is therefore likely to be highly system dependent, with the largest benefit being in systems where the edges of the heterocycles are accessible to CO₂, for example, MFM-18X,²⁸ NOTT-122,⁴³ and the quinoxaline-based MOFs of Zhu and co-workers.⁴⁴ It is notable that while three quinoxaline MOFs were reported, considerably enhanced CO₂ uptake was observed in the only MOF in which the edges of the pyrazine system were accessible.

Comparison of the relative binding strengths of CH₄ and CO₂ indicates that any of the carbocyclic linkers studied in this work are suitable for selective adsorption of CO₂ over CH₄ at low pressure but that the presence of at least one central

aromatic ring improves selectivity considerably over the single unsaturated C–C bond present in L0_c. Comparison of the heterocyclic and carbocyclic linkers suggests that while the presence of heteroatoms can greatly enhance the selectivity toward CO₂ for systems in which the edges of the heterocyclic rings are accessible, the presence of heteroatoms tends to favor methane in regions directly above and below the heterocyclic rings, and the incorporation of heteroatoms into ligands in which the heteroatom is not able to interact directly with CO₂ may, in fact, reduce the selectivity of the MOF for carbon dioxide over methane at low pressure.

ASSOCIATED CONTENT

Supporting Information

The Supporting Information is available free of charge on the ACS Publications website at DOI: 10.1021/acs.jpcc.6b08767.

Calculation of pore size distribution; additional CH₄ binding sites on L4_c, L5_c, and L5_h; additional CO₂ binding sites on L3_c and L5_c; CHELPG charges for L3_h and L3_c (PDF)

AUTHOR INFORMATION

Corresponding Author

*E-mail Elena.Besley@nottingham.ac.uk (E.B.).

ORCID

Elena Besley: 0000-0002-9910-7603

Notes

The authors declare no competing financial interest.

ACKNOWLEDGMENTS

The authors acknowledge funding from EPSRC and the University of Nottingham High Performance Computing facility for computational time; E.B. acknowledges an ERC Consolidator Grant for financial support. We are grateful to Dr. Alexander Markevich for providing benchmarking calculations for the CO₂–benzene dimer.

REFERENCES

- (1) Batten, S. R.; Champness, N. R.; Chen, X. M.; Garcia-Martinez, J.; Kitagawa, S.; Ohmstrom, L.; O'Keeffe, M.; Suh, M. P.; Reedijk, J. Terminology of Metal-Organic Frameworks and Coordination Polymers (Iupac Recommendations 2013). *Pure Appl. Chem.* **2013**, *85*, 1715–1724.
- (2) Rowsell, J. L. C.; Yaghi, O. M. Metal-Organic Frameworks: A New Class of Porous Materials. *Microporous Mesoporous Mater.* **2004**, *73*, 3–14.
- (3) Yaghi, O. M.; O'Keeffe, M.; Ockwig, N. W.; Chae, H. K.; Eddaoudi, M.; Kim, J. Reticular Synthesis and the Design of New Materials. *Nature* **2003**, *423*, 705–714.
- (4) Lu, W. G.; et al. Tuning the Structure and Function of Metal-Organic Frameworks Via Linker Design. *Chem. Soc. Rev.* **2014**, *43*, 5561–5593.
- (5) Allendorf, M. D.; Stavila, V. Crystal Engineering, Structure-Function Relationships, and the Future of Metal-Organic Frameworks. *CrystEngComm* **2015**, *17*, 229–246.
- (6) Bae, Y. S.; Snurr, R. Q. Development and Evaluation of Porous Materials for Carbon Dioxide Separation and Capture. *Angew. Chem., Int. Ed.* **2011**, *50*, 11586–11596.
- (7) Li, J. R.; Kuppler, R. J.; Zhou, H. C. Selective Gas Adsorption and Separation in Metal-Organic Frameworks. *Chem. Soc. Rev.* **2009**, *38*, 1477–1504.
- (8) Chen, S. Q.; Zhai, Q. G.; Li, S. N.; Jiang, Y. C.; Hu, M. C. Channel Partition into Nanoscale Polyhedral Cages of a Triple-Self-

Interpenetrated Metal-Organic Framework with High CO₂ Uptake. *Inorg. Chem.* **2015**, *54*, 10–12.

- (9) Yazaydin, A. O.; et al. Screening of Metal-Organic Frameworks for Carbon Dioxide Capture from Flue Gas Using a Combined Experimental and Modeling Approach. *J. Am. Chem. Soc.* **2009**, *131*, 18198.
- (10) Eddaoudi, M.; Kim, J.; Rosi, N.; Vodak, D.; Wachter, J.; O'Keeffe, M.; Yaghi, O. M. Systematic Design of Pore Size and Functionality in Isoreticular MOFs and Their Application in Methane Storage. *Science* **2002**, *295*, 469–472.
- (11) Peng, Y.; Krungleviciute, V.; Eryazici, I.; Hupp, J. T.; Farha, O. K.; Yildirim, T. Methane Storage in Metal-Organic Frameworks: Current Records, Surprise Findings, and Challenges. *J. Am. Chem. Soc.* **2013**, *135*, 11887–11894.
- (12) Gandara, F.; Furukawa, H.; Lee, S.; Yaghi, O. M. High Methane Storage Capacity in Aluminum Metal-Organic Frameworks. *J. Am. Chem. Soc.* **2014**, *136*, 5271–5274.
- (13) Rana, M. K.; Koh, H. S.; Zuberi, H.; Siegel, D. J. Methane Storage in Metal-Substituted Metal-Organic Frameworks: Thermodynamics, Usable Capacity, and the Impact of Enhanced Binding Sites. *J. Phys. Chem. C* **2014**, *118*, 2929–2942.
- (14) Colon, Y. J.; Snurr, R. Q. High-Throughput Computational Screening of Metal-Organic Frameworks. *Chem. Soc. Rev.* **2014**, *43*, 5735–5749.
- (15) Duren, T.; Bae, Y. S.; Snurr, R. Q. Using Molecular Simulation to Characterise Metal-Organic Frameworks for Adsorption Applications. *Chem. Soc. Rev.* **2009**, *38*, 1237–1247.
- (16) Gomez-Gualdron, D. A.; Gutov, O. V.; Krungleviciute, V.; Borah, B.; Mondloch, J. E.; Hupp, J. T.; Yildirim, T.; Farha, O. K.; Snurr, R. Q. Computational Design of Metal-Organic Frameworks Based on Stable Zirconium Building Units for Storage and Delivery of Methane. *Chem. Mater.* **2014**, *26*, 5632–5639.
- (17) Wilmer, C. E.; Leaf, M.; Lee, C. Y.; Farha, O. K.; Hauser, B. G.; Hupp, J. T.; Snurr, R. Q. Large-Scale Screening of Hypothetical Metal-Organic Frameworks. *Nat. Chem.* **2012**, *4*, 83–89.
- (18) Bichoutskaia, E.; Suyetin, M.; Bound, M.; Yan, Y.; Schroeder, M. Methane Adsorption in Metal-Organic Frameworks Containing Nanographene Linkers: A Computational Study. *J. Phys. Chem. C* **2014**, *118*, 15573–15580.
- (19) Fernandez, M.; Woo, T. K.; Wilmer, C. E.; Snurr, R. Q. Large-Scale Quantitative Structure-Property Relationship (QsPr) Analysis of Methane Storage in Metal-Organic Frameworks. *J. Phys. Chem. C* **2013**, *117*, 7681–7689.
- (20) Grajciar, L.; Nachtigall, P.; Bludsky, O.; Rubes, M. Accurate Ab Initio Description of Adsorption on Coordinatively Unsaturated Cu²⁺ and Fe³⁺ Sites in MOFs. *J. Chem. Theory Comput.* **2015**, *11*, 230–238.
- (21) Haldoupis, E.; Borycz, J.; Shi, H. L.; Vogiatzis, K. D.; Bai, P.; Queen, W. L.; Gagliardi, L.; Siepmann, J. I. Ab Initio Derived Force Fields for Predicting CO₂ Adsorption and Accessibility of Metal Sites in the Metal-Organic Frameworks M-MOF-74 (M = Mn, Co, Ni, Cu). *J. Phys. Chem. C* **2015**, *119*, 16058–16071.
- (22) Koh, H. S.; Rana, M. K.; Wong-Foy, A. G.; Siegel, D. J. Predicting Methane Storage in Open-Metal-Site Metal-Organic Frameworks. *J. Phys. Chem. C* **2015**, *119*, 13451–13458.
- (23) Chen, L. J.; Grajciar, L.; Nachtigall, P.; Duren, T. Accurate Prediction of Methane Adsorption in a Metal-Organic Framework with Unsaturated Metal Sites by Direct Implementation of an Ab Initio Derived Potential Energy Surface in Gcmc Simulation. *J. Phys. Chem. C* **2011**, *115*, 23074–23080.
- (24) Torrisi, A.; Bell, R. G.; Mellot-Draznieks, C. Predicting the Impact of Functionalized Ligands on CO₂ Adsorption in MOFs: A Combined DFT and Grand Canonical Monte Carlo Study. *Microporous Mesoporous Mater.* **2013**, *168*, 225–238.
- (25) Torrisi, A.; Mellot-Draznieks, C.; Bell, R. G. Impact of Ligands on CO₂ Adsorption in Metal-Organic Frameworks: First Principles Study of the Interaction of CO₂ with Functionalized Benzenes. II. Effect of Polar and Acidic Substituents. *J. Chem. Phys.* **2010**, *132*, 044705.
- (26) Alsmail, N. H.; et al. Analysis of High and Selective Uptake of CO₂ in an Oxamide-Containing {Cu₂(Oocr)(4)}-Based Metal-Organic Framework. *Chem. - Eur. J.* **2014**, *20*, 7317–7324.
- (27) Yu, D.; Matteucci, S.; Stangland, E.; Calverley, E.; Wegener, H.; Anaya, D. Quantum Chemistry Calculation and Experimental Study of CO₂/CH₄ and Functional Group Interactions for the Design of Solubility Selective Membrane Materials. *J. Membr. Sci.* **2013**, *441*, 137–147.
- (28) Moreau, F.; et al. Engineering Porosity and Rotational Dynamics in a Series of Octacarboxylate Metal-Organic Frameworks. *Proc. Natl. Acad. Sci. U. S. A.* Submitted.
- (29) Goerigk, L.; Grimme, S. A Thorough Benchmark of Density Functional Methods for General Main Group Thermochemistry, Kinetics, and Noncovalent Interactions. *Phys. Chem. Chem. Phys.* **2011**, *13*, 6670–6688.
- (30) Shao, Y. H.; et al. Advances in Molecular Quantum Chemistry Contained in the Q-Chem 4 Program Package. *Mol. Phys.* **2015**, *113*, 184–215.
- (31) Fischer, M.; Gomes, J. R. B.; Froba, M.; Jorge, M. Modeling Adsorption in Metal-Organic Frameworks with Open Metal Sites: Propane/Propylene Separations. *Langmuir* **2012**, *28*, 8537–8549.
- (32) Fischer, M.; Hoffmann, F.; Froba, M. Molecular Simulation of Hydrogen Adsorption in Metal-Organic Frameworks. *Colloids Surf, A* **2010**, *357*, 35–42.
- (33) Becke, A. D. Density-Functional Thermochemistry 0.3. The Role of Exact Exchange. *J. Chem. Phys.* **1993**, *98*, 5648–5652.
- (34) Boys, S. F.; Bernardi, F. Calculation of Small Molecular Interactions by Differences of Separate Total Energies - Some Procedures with Reduced Errors. *Mol. Phys.* **1970**, *19*, 553.
- (35) Breneman, C. M.; Wiberg, K. B. Determining Atom-Centered Monopoles from Molecular Electrostatic Potentials - the Need for High Sampling Density in Formamide Conformational-Analysis. *J. Comput. Chem.* **1990**, *11*, 361–373.
- (36) Witte, J.; Neaton, J. B.; Head-Gordon, M. Assessing Electronic Structure Approaches for Gas-Ligand Interactions in Metal-Organic Frameworks: The CO₂-Benzene Complex. *J. Chem. Phys.* **2014**, *140*, 104707.
- (37) Vogiatzis, K. D.; Klopffer, W.; Friedrich, J. Non-Covalent Interactions of CO₂ with Functional Groups of Metal-Organic Frameworks from a Ccsd(T) Scheme Applicable to Large Systems. *J. Chem. Theory Comput.* **2015**, *11*, 1574–1584.
- (38) Supronowicz, B.; Mavrandonakis, A.; Heine, T. Interaction of Small Gases with the Unsaturated Metal Centers of the HKUST-1 Metal Organic Framework. *J. Phys. Chem. C* **2013**, *117*, 14570–14578.
- (39) Chen, L.; Cao, F.; Sun, H. Ab Initio Study of the π - π Interactions between CO₂ and Benzene, Pyridine, and Pyrrole. *Int. J. Quantum Chem.* **2013**, *113*, 2261–2266.
- (40) Henley, A.; Bound, M.; Besley, E. Effective Binding of Methane Using a Weak Hydrogen Bond. *J. Phys. Chem. A* **2016**, *120*, 3701–3709.
- (41) Wang, T. C.; et al. Ultrahigh Surface Area Zirconium MOFs and Insights into the Applicability of the BET Theory. *J. Am. Chem. Soc.* **2015**, *137*, 3585–3591.
- (42) Farha, O. K.; Eryazici, I.; Jeong, N. C.; Hauser, B. G.; Wilmer, C. E.; Sarjeant, A. A.; Snurr, R. Q.; Nguyen, S. T.; Yazaydin, A. Ö.; Hupp, J. T. Metal-Organic Framework Materials with Ultrahigh Surface Areas: Is the Sky the Limit? *J. Am. Chem. Soc.* **2012**, *134*, 15016–15021.
- (43) Yan, Y.; Suyetin, M.; Bichoutskaia, E.; Blake, A. J.; Allan, D. R.; Barnett, S. A.; Schroder, M. Modulating the Packing of Cu-24(Isophthalate)(24) Cuboctahedra in a Triazole-Containing Metal-Organic Polyhedral Framework. *Chem. Sci.* **2013**, *4*, 1731–1736.
- (44) Zhu, Y.; Wang, Y. M.; Zhao, S. Y.; Liu, P.; Wei, C.; Wu, Y. L.; Xia, C. K.; Xie, J. M. Three N-H Functionalized Metal-Organic Frameworks with Selective CO₂ Uptake, Dye Capture, and Catalysis. *Inorg. Chem.* **2014**, *53*, 7692–7699.